Supergiant fast X-ray transients as an under-luminous class of supergiant X-ray binaries

E. Bozzo*

ISDC, University of Geneva, Chemin dÉcogia 16, CH-1290 Versoix, Switzerland

P. Romano

INAF, Istituto di Astrofisica Spaziale e Fisica Cosmica - Palermo, via U. La Malfa 153, 90146 Palermo, Italy

L. Ducci

Institut für Astronomie und Astrophysik, Eberhard Karls Universität, Sand 1, 72076 Tübingen, Germany; ISDC, University of Geneva, Chemin dÉcogia 16, CH-1290 Versoix, Switzerland

F. Bernardini

Department of Physics & Astronomy, Wayne State University, 666 W. Hancock St., Detroit, MI 48201, USA; INAF, Osservatorio Astronomico di Capodimonte, Salita Moiariello 16, I-80131 Napoli, Italia

M. Falanga

International Space Science Institute, Hallerstrasse 6, CH-3012 Bern, Switzerland; International Space Science Institute in Beijing, No. 1 Nan Er Tiao, Zhong Guan Cun, Beijing 100190, China.

Abstract

The usage of cumulative luminosity distributions, constructed thanks to the long-term observations available through wide field hard X-ray imagers, has been recently exploited to study the averaged high energy emission (>17 keV) from Supergiant Fast X-ray Transients (SFXTs) and classical Supergiant High Mass X-ray Binaries (SgXBs). Here, we take advantage of the long term monitorings now available with *Swift*/XRT to construct for the first time the cumulative luminosity distributions of a number of SFXTs and the classical SgXB IGR J18027-2016 in the soft X-ray domain with a high sensitivity focusing X-ray telescope (0.3-10 keV).

By complementing previous results obtained in the hard X-rays, we found that classical SgXBs are characterized by cumulative distributions with a single knee around $\sim 10^{36}$-10^{37} erg s^{-1}, while SFXTs are found to be systematically sub-luminous and their distributions are shifted at significantly lower luminosities (a factor of ~10-100). As the luminosity states in which these sources spend most of their time are typically below the sensitivity limit of large field of view hard X-ray imagers, we conclude that soft X-ray monitorings carried out with high sensitivity telescopes are particularly crucial to reconstruct the complete profile of the SFXT cumulative luminosity distributions.

The difference between the cumulative luminosity distributions of classical SgXBs and SFXTs is interpreted in terms of accretion from a structured wind in the former sources and the presence of magnetic/centrifugal gates or a quasi-spherical settling accretion regime in the latter.

Keywords: neutron star, accretion, X-ray binaries, high mass X-ray binaries, IGR J18027-2016

1. Introduction

Most of the so-called "classical" Supergiant X-ray binaries (SgXBs) host a neutron star (NS) accreting material from the wind of its O-B supergiant companion. These sources are characterized by a nearly persistent X-ray luminosity of $L_X = 10^{35}$-10^{37} erg s^{-1} (mostly depending on their orbital period) and display variations in the X-ray intensity by as large as a factor of ~20-50 on time scales of hundreds to thousands of seconds. This pronounced variability is usually ascribed to the presence of inhomogeneities in the accreting medium ("clumps"; see, e.g., Negueruela et al., 2006, and references therein). Orbital periods measured for many of these systems range from a few to tens of days (see, e.g., Chaty, 2013, for a recent review). The presence of neutron stars could be firmly established in several cases thanks to the detection of X-ray pulsations (Liu et al., 2006). Measured spin periods are typically long, spanning from tens to several thousand seconds. Such slow rotations are as-

*Corresponding author

Email addresses: enrico.bozzo@unige.ch (E. Bozzo), romano@ifc.inaf.it (P. Romano), Lorenzo.Ducci@unige.ch (L. Ducci), fh0126@wayne.edu (F. Bernardini), mfalanga@issibern.ch (M. Falanga)

cribed to the effect of torque due to the wind accretion process (see, e.g., Shakura et al., 2013, and references therein).

Supergiant Fast X-ray transients (SFXTs) are a sub-class of SgXBs (Ducci et al., 2014), sharing a number of similar properties with classical systems (e.g., similar orbital periods; Bozzo et al., 2013) but displaying a much more pronounced variability in the X-ray domain. These sources spend most of their time in low luminosity states ($L_X = 10^{32}$-10^{33} erg s^{-1}) and only sporadically undergo few hours-long outbursts reaching peak luminosities comparable to the persistent level of other SgXBs (Sguera et al., 2006). The criterion proposed to distinguish between classical systems and SFXTs is based on the larger dynamical range achieved by the latter sources. In particular, a source is classified as "intermediate SFXT" if a variability as large as a factor of $\gtrsim$100 is recorded in the X-ray domain, and a proper SFXT if the dynamic range is significantly above this value (see, e.g., Romano et al., 2014b, hereafter R14). Among all the known SFXTs, three of them displayed the largest dynamic range ($\geq 10^4$-10^5) and we thus refer to them from now onward as "SFXT prototypes". These three sources are: IGR J08408-4532, XTE J1739-302, and IGR J17544-2619.

As inhomogeneities in the accreting material are not sufficient to account for the SFXT pronounced variability, the mechanism regulating the activity of these source is still a matter of debate (see, e.g., Bozzo et al., 2013; Chaty, 2013). Only in a few cases X-ray pulsations firmly established the presence of neutron stars in SFXTs, but the similarity of their X-ray spectra with those of other accreting neutron star systems convincingly led to the conclusion that SFXTs should also host the same kind of compact objects (Negueruela et al., 2006).

Large field-of-view (FoV) hard X-ray imagers, like the IBIS/ISGRI on-board *INTEGRAL* (20 keV-1 MeV; Ubertini et al., 2003; Lebrun et al., 2003) and the BAT on-board *Swift* (15-150 keV; Barthelmy et al., 2005), have been very efficient in catching a large number of sporadic SFXT outbursts and proved particularly well suited to study the brightest luminosity states achieved by these sources ($\gtrsim 10^{35}$ erg s^{-1}; see, e.g., Romano et al., 2014a). The long-term monitoring data now available have been exploited to estimate the SFXT activity duty-cycle (DC; see, e.g., R14; Paizis & Sidoli, 2014, hereafter P14). The latter was found to be significantly lower (1-5 %) in the hard X-ray domain than that of classical SgXBs ($\gtrsim$80 %). By using all archival ISGRI data, P14 also reported a detailed comparison between the cumulative luminosity distributions of these two classes of sources. They showed that in the energy range 17-50 keV the distributions of SFXTs can be reasonably well described by a single power-law, while those of classical SgXBs are typically more complex, showing a knee at luminosities $\sim 10^{36}$ erg s^{-1} and requiring at least two different power-laws to satisfactorily describe their profiles.

The fainter states of SFXTs can be accurately studied only by using pointed observations with focusing X-ray telescopes. Among these, XRT (Burrows et al., 2005) on-board *Swift* (Gehrels et al., 2004) proved to be particularly useful in carrying out long-term monitoring of the SFXTs, as it can take advantage of the unique scheduling flexibility of the *Swift* satellite. For most of the SFXTs, observations lasting 1 ks and achieving a limiting sensitivity comparable to the lowest emission level of these sources have been carried out twice a week from 2007 to present (Sidoli et al., 2008; Romano et al., 2009, 2011; Romano et al., 2014b). These data provide now a sufficiently long baseline to be compared with the results obtained through wide FoV hard X-ray imagers. A first comparison was reported by R14. These authors showed that XRT data allow us to extend the estimation of the SFXT DC across 2 orders of magnitude more in X-ray luminosity compared to large FoV hard X-ray instruments. Their main finding is that a DC comparable to that of classical systems ($\gtrsim$70-80%) is recovered for the SFXTs when luminosities as low as $\sim 10^{32}$-10^{33} erg s^{-1} can be probed as lower limit for the calculation of the DC.

In this paper, we make use of the same XRT dataset as reported by R14 to construct the cumulative luminosity distributions of most of the currently known SFXT sources. We also present the analysis of the still unpublished XRT data of IGR J18027-2016, a classical SgXB monitored for a sufficiently long time with XRT to build a meaningful cumulative luminosity distribution. We compare the cumulative luminosity distributions of SFXTs and classical SgXBs available so far in the hard and soft X-rays, providing an interpretation for the two classes of objects in terms of different wind accretion scenarios.

Table 1: Overview of the XRT data used in this work. Exp. is the total exposure time available for each source.

Source	Campaign Start (UTC)	End (UTC)	Exp. (ks)
SFXTs			
IGR J08408-4503	2011-10-20	2012-08-05	74.4
IGR J16328-4726	2011-10-20	2013-10-24	88.0
IGR J16418-4532[a]	2011-02-18	2011-07-30	43.3
IGR J16465-4507[a]	2013-01-20	2013-09-01	58.6
IGR J16479-4514	2007-10-26	2009-10-25	159.8
IGR J17354-3255	2012-07-18	2012-07-28	23.7
XTE J1739-302	2007-10-27	2009-11-01	206.6
IGR J17544-2619	2007-10-28	2009-11-03	142.5
AX J1841.0-0536	2007-10-26	2008-11-15	96.5
IGR J18483-0311	2009-06-11	2009-07-08	44.1
Classical SgXBs			
IGR J18027-2016	2012-06-07	2012-09-01	53.6

[a]: These sources have been recently suggested to be classical SgXBs and not SFXTs. Our analysis further support this change in their classification (see Sect. 4)

2. *Swift* sample and data analysis

In order to produce the cumulative luminosity distributions of the currently known SFXTs, we made use of all available

XRT data collected from 2007 to 2013 from the 10 sources listed in Table 1. This data-set is the same that has been presented by R14. It comprises:

- data from the monitoring of the SFXTs IGR J16479-4514, XTE J1739-302, and IGR J17544-2619 carried out from 2007 October 26 to 2009 November 03;
- data from the monitoring of AX J1841.0-0536 obtained from 2007 October 26 to 2008 November 15;
- data from the monitoring of one complete orbit of the SFXTs IGR J18483-0311 (collected from 2009 June 11 to 2009 July 08), IGR J16418-4532 (carried out from 2011 February 18 to 2011 July 30), and IGR J17354-3255 (carried out from 2012 July 18 to 2012 July 28);
- data accumulated during the most recent monitoring campaigns of the SFXTs IGR J08408-4503, IGR J16328-4726, and IGR J16465-4507. These campaigns have been carried out from 2011 October 20 to 2013 October 24.

All the details about the specific XRT pointings used for the different sources and the analysis technique have been exhaustively reported by R14. We thus refer the reader to that paper for further information and do not repeat them here.

The only previously known classical SgXBs that has been monitored for at least one complete orbital period with XRT (thus with comparable strategy as the previous campaigns) is IGR J18027-2016. We thus included in the present data-set all XRT observations performed in the direction of the source. As these data have not been reported elsewhere, we provide in Table 2 all the relevant details on the available XRT pointings and describe briefly the XRT data analysis technique in Sect. 2.1. We also provide there a summary of our present knowledge on IGR J18027-2016.

2.1. The classical SgXB IGR J18027-2016

IGR J18027-2016 is a classical SgXBs with an orbital period of 4.57 days. The presence of an accreting NS in this system was confirmed by the detection of pulsations at 139.47 s (Hill et al., 2005). The source undergoes regular X-ray eclipses and features a typical X-ray variability by a factor of 10-50 as expected for a classical SgXB (Walter et al., 2006). The companion star is a B0-BI supergiant located at a distance of 12.4 kpc (Mason et al., 2011). This source is well suited to be monitored by XRT as its average X-ray flux (a few 10^{-11} erg cm^{-2} s^{-1}) is low enough to cause only a moderate pile-up and at the same time its X-ray emission can be reasonably well characterized by short pointings of 1-2 ks. The XRT monitoring campaign covered 7 orbital periods of the source with daily pointings of 1–2 ks in Photon counting (PC) mode. From the XRT online tool[1] we first obtained the most accurate source position to date for this source at RA(J2000) = 270.67494, Dec(J2000) = −20.28813, with an estimated uncertainty of 1.4 arcsec radius (90 % c.l.; Evans et al., 2009).

[1] http://www.swift.ac.uk/user_objects/

Table 2: Log of the XRT observations carried out in the direction of IGR J18027-2016. All data have been collected in PC mode.

Sequence	Start time (UT) (yyyy-mm-dd hh:mm:ss)	End time (UT) (yyyy-mm-dd hh:mm:ss)	Exposure (s)
00035720005	2012-06-07 05:51:33	2012-06-07 23:41:57	1409
00035720006	2012-06-08 00:58:39	2012-06-08 02:52:57	1880
00035720007	2012-06-09 02:41:46	2012-06-09 04:28:55	1452
00035720008	2012-06-10 01:04:53	2012-06-10 02:59:56	2028
00035720009	2012-06-11 05:51:49	2012-06-11 20:27:57	1901
00035720010	2012-06-18 11:20:49	2012-06-18 15:55:56	1419
00035720011	2012-06-20 15:56:19	2012-06-20 17:39:57	878
00035720012	2012-06-21 03:28:46	2012-06-21 11:40:56	1126
00035720013	2012-06-22 00:18:45	2012-06-22 08:28:58	2179
00035720014	2012-07-05 10:38:33	2012-07-05 12:10:54	1928
00035720015	2012-07-10 20:35:19	2012-07-10 22:15:54	1885
00035720016	2012-07-16 09:22:25	2012-07-16 12:49:55	1863
00035720017	2012-07-17 04:38:15	2012-07-17 08:14:55	2043
00035720018	2012-07-18 17:46:13	2012-07-18 19:30:55	1906
00035720019	2012-07-20 01:25:06	2012-07-20 06:24:55	1236
00035720020	2012-08-01 05:35:59	2012-08-01 07:19:55	1963
00035720021	2012-08-02 18:22:27	2012-08-02 20:17:54	1978
00035720022	2012-08-03 16:45:30	2012-08-03 18:40:55	1968
00035720023	2012-08-04 18:28:18	2012-08-04 18:43:54	933
00035720024	2012-08-05 03:53:21	2012-08-05 05:46:55	2101
00035720025	2012-08-16 06:10:00	2012-08-16 07:54:56	2151
00035720026	2012-08-17 14:32:42	2012-08-17 16:02:55	2043
00035720027	2012-08-18 22:19:51	2012-08-18 23:59:55	1921
00035720028	2012-08-19 12:45:48	2012-08-19 13:11:40	1529
00035720029	2012-08-20 11:31:10	2012-08-20 13:26:54	1976
00035720030	2012-08-28 10:03:02	2012-08-28 11:54:55	1983
00035720031	2012-08-29 00:27:41	2012-08-29 02:25:56	2046
00035720032	2012-08-30 02:12:07	2012-08-30 03:59:56	1873
00035720033	2012-08-31 02:15:41	2012-08-31 04:15:56	1996
00035720034	2012-09-01 04:02:49	2012-09-01 06:01:56	2033

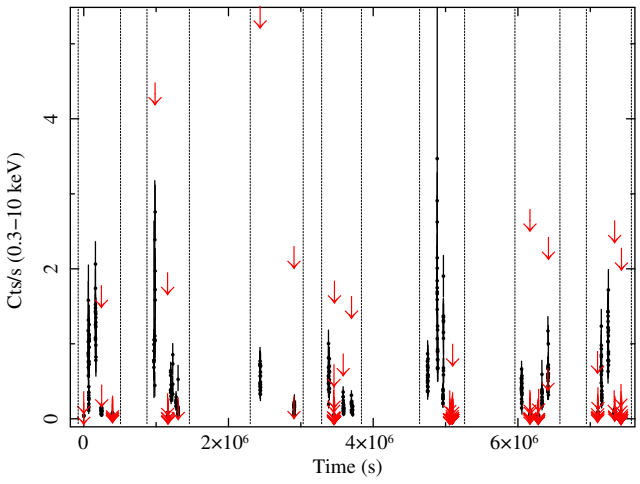

Figure 1: XRT lightcurve of IGR J18027-2016 in the 0.3-10 keV energy band. The bin time of the lightcurve is 100 s. The source count-rate estimated in the time bins where a detection above 3 σ was achieved is represented in black, together with the corresponding uncertainty. Upper limits on the source non-detection are indicated with red arrows. The 7 orbital periods of the source monitored by XRT are separated by vertical dashed lines.

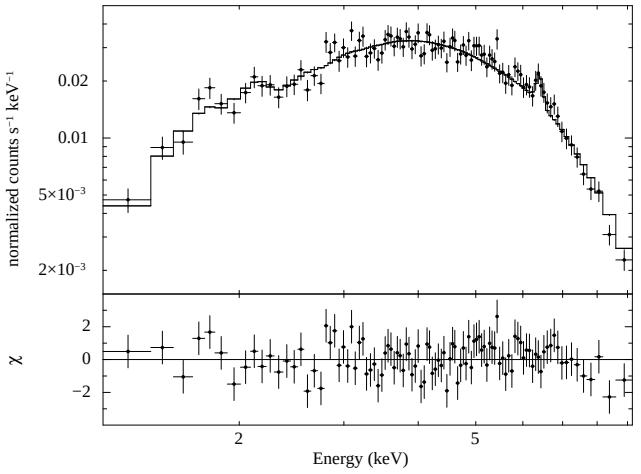

Figure 2: The average XRT spectrum of IGR J18027-2016 grouped in oder to have at least 70 photons per energy bin. The best fit to the spectrum is obtained by using a simple absorbed power-law model plus a gaussian thin line at ~6.4 keV (see Sect. 2.1 for details). The residuals from the fit are shown in the bottom panel.

The 0.3–10 keV background-subtracted lightcurve (100 s resolution) of the source is shown in Fig. 1. The source XRT spectrum accumulated over all available data and rebinned to have at least 70 photons per energy bin is reported in Fig. 2. The latter could be fit ($\chi^2_{\rm red}$/d.o.f. = 1.12/100) by using a simple absorbed power-law model with a column density of (2.6 ± 0.2) × 10^{22} cm^{-2} and a photon index of Γ = 0.43±0.09. We found some evidence for the presence of an emission Fe Kα line around 6.4 keV. If added to the fit ($\chi^2_{\rm red}$/d.o.f. = 0.97/98), the estimated centroid energy would be 6.39±0.06 keV and the corresponding equivalent width 0.1 keV. Similar spectral features are commonly observed in the X-ray spectra of SgXBs, and are usually ascribed to the scattering of X-rays on the wind material surrounding the neutron star (Torrejon et al., 2011).

The average source count-rate as recorded by XRT was 0.17 cts s^{-1}, corresponding to a 2-10 keV absorbed X-ray flux of 5.6×10^{-11} erg cm^{-2} s^{-1}. The unabsorbed X-ray flux estimated by assuming the above spectral model is 6.3×10^{-11} erg cm^{-2} s^{-1}.

For completeness, we report in Fig. 3 the folded *Swift*/BAT lightcurve, as retrieved from the instrument transient monitoring (Krimm et al., 2013) page[2]. These data cover the period 53415.9874 - 56930.0114 MJD. We used the ephemerides provided by Hill et al. (2005). We also show in the same figure the *Swift*/XRT lightcurve folded with the same ephemerides and the orbital phase coverage of our XRT monitoring program. The presence of the X-ray eclipse is evident in both XRT and BAT folded lightcurves, in agreement with previous results (Hill et al., 2005). A more detailed analysis of these data is beyond the scope of the present work and will be reported else-

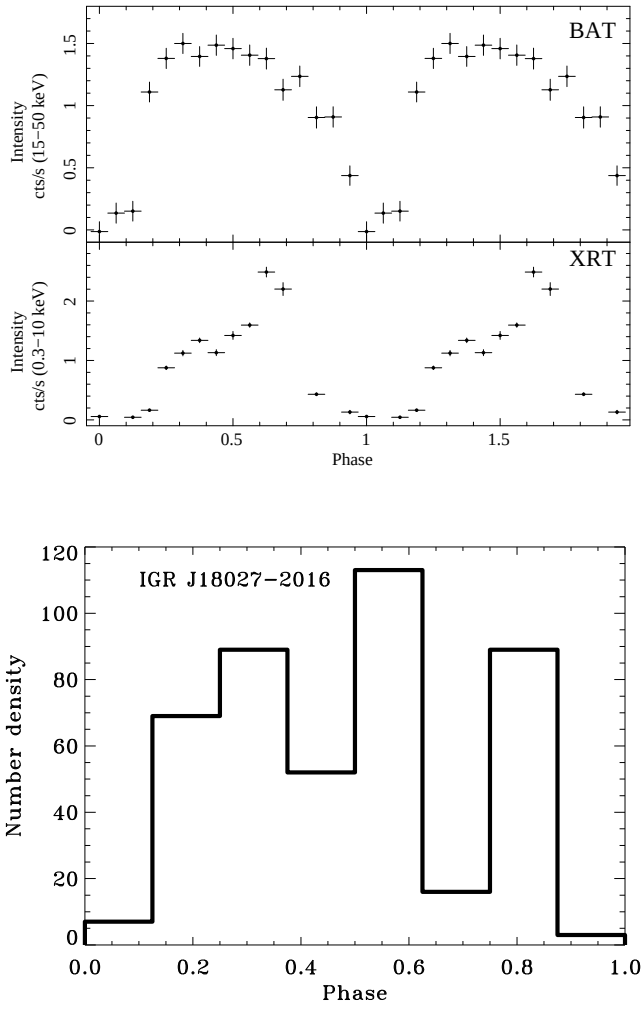

Figure 3: *Upper panel*: Folded *Swift*/BAT lightcurve of IGR J18027-2016 in the 15-150 keV energy range, as retrieved from the instrument transients monitoring page (see Sect. 2.1 for details). *Middle panel*: XRT lightcurve shown in Fig. 1 and folded on the source orbital period. *Bottom panel*: Orbital phase coverage of the XRT monitoring observations of IGR J18027-2016. The units on the y-axis give the number of time bins in Fig. 1 available for each phase. In all panels we used an orbital period of 4.5696 ± 0.0009 days and an ephemeris for the mid-eclipse of $T_{\rm mid}$ = 52931.37 ± 0.04 MJD (Hill et al., 2005).

[2]See http://swift.gsfc.nasa.gov/results/transients/weak/IGRJ18027-2016/

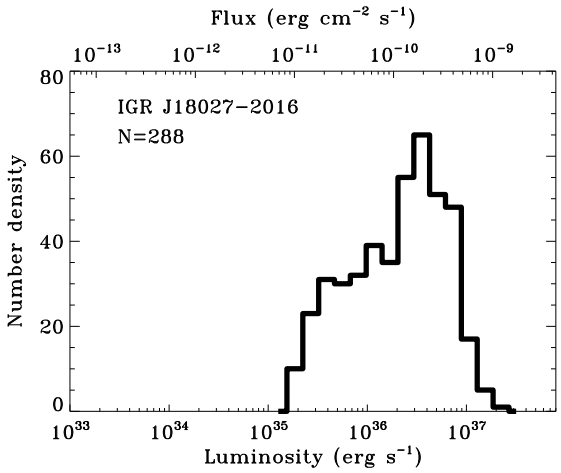

Figure 4: Distributions of the XRT luminosity (lower axis) and unabsorbed flux (upper axis) of IGR J18027-2016 as obtained from the source lightcurve binned at 100 s (2-10 keV).

where. Figure 4 presents the distribution of the source XRT luminosity and unabsorbed flux (2-10 keV) as obtained from the XRT light curves binned at 100 s. Similar distributions have been discussed by R14 for the entire sample of the SFXTs observed by XRT, and illustrate how many times each object is detected at a certain flux or luminosity during the XRT campaign.

3. XRT cumulative luminosity distributions

We created the cumulative luminosity distributions of all sources considered in this work by using the corresponding XRT lightcurves binned at 100 s. Observations where a significant detection of the source ($\geq 3\ \sigma$) was not achieved in 100 s were excluded from further analysis (including time intervals corresponding to X-ray eclipses, where relevant). For all SFXTs, we used the same distances as R14 to convert from count-rates to luminosity and the 2-10 keV unabsorbed flux of each source. The conversion for IGR J18027-2016 was calculated by adopting the parameters obtained from the fit to the mean source spectrum (see Sect. 2.1). The cumulative luminosity distributions of all SFXTs that have been monitored at least for one orbital period by XRT and that of IGR J18027-2016 are shown in Fig. 5 with 100 bins per decade in luminosity. We need to distinguish the following cases: (i) IGR J16479−4514, XTE J1739−302, and IGR J17544−2619 went into outburst during the corresponding observing campaigns, so the data shown in the left panel of Fig. 5 include all luminosity levels experienced by these sources; (2) IGR J08408−4503, IGR J16328−4726, and AX J1841.0−0536 did not experience an outburst during the monitoring, but outbursts were recorded at different times (R14). To assess their overall distributions, we thus also added the data of such outbursts and plot the corresponding distributions in the right panel of Fig. 5. This does not affect our conclusions.

All cumulative luminosity distributions in Fig. 5 were also normalized to the total exposure time of each source, such that the source DC correspond to the highest value on the y-axis and an easier comparison can be carried out with the cumulative distributions obtained in the hard X-rays (P14). By comparing our Fig. 5 with Fig. 1 in P14, we first notice that the cumulative distributions of SFXTs in the soft X-rays do not have power-law shaped profiles. More precisely:

- the source IGR J18027-2016 is characterized by a cumulative distribution with a single knee around 10^{36} erg s^{-1}, as expected for classical SgXBs.

- the distributions of IGR J16465-4507 and IGR J16418-4532 closely resemble those of classical SgXBs. In the logN-logL plot, a knee is observed at a certain critical luminosity and the slope of the profile changes abruptly above this value. Similar profiles were observed by P14 in the cases of Vela X-1 and 4U 1700-377. The only difference seems to be that the IGRs mentioned above are at a distance much larger than that of Vela X-1 and 4U 1700-377. Their fluxes are thus too low (by a factor of $\gtrsim$100) for the wide FoV instruments to exploit their entire X-ray dynamical range. The higher sensitivity of XRT allows us to follow more accurately their activity and the complete profile is recovered. Interestingly, IGR J16465-4507 and IGR J16418-4532 have been recently classified as classical SgXBs rather than SFXTs by R14 and Drave et al. (2013), respectively. Our results support this reclassification, and thus these two sources should be considered from now onward as part of the classical SgXBs. The cumulative luminosity distributions of all classical SgXBs in Fig. 5 have been plot with thicker dashed lines.

- IGR J18483-0311 and IGR J17354-3255 have similar distributions as classical SgXBs, but their overall profile and the knees appear to be shifted at lower luminosities ($\sim 10^{35}$ erg s^{-1}). These two sources are classified as "intermediate" SFXTs, and are thus thought to be the missing link between the SFXTs and classical SgXBs (due to their reduced dynamic range in the X-ray luminosity; see, e.g., Rahoui & Chaty, 2008; Giunta et al., 2009; Liu et al., 2011; Ducci et al., 2013). The cumulative luminosity distributions of these two sources have been plotted in Fig. 5 by using dot-dashed lines.

- A similar conclusion as above applies to the cumulative luminosity distributions of the SFXTs IGR J16479-4514, IGR J16328-4726, and AX J1841.0-0536. The reduction in the average luminosity of IGR J16479-4514 and IGR J16328-4726 is evident once a comparison is carried out with, e.g., IGR J16418-4532 in the present paper and Vela X-1 in P14, respectively (note that Vela X-1 as an orbital period close to IGR J16328-4726, while IGR J16418-4532 has a period similar to IGR J16479-4514). No orbital period is known yet in the case of AX J1841.0-0536. The cumulative luminosity distributions of these SFXTs are plot in Fig. 5 with dotted lines.

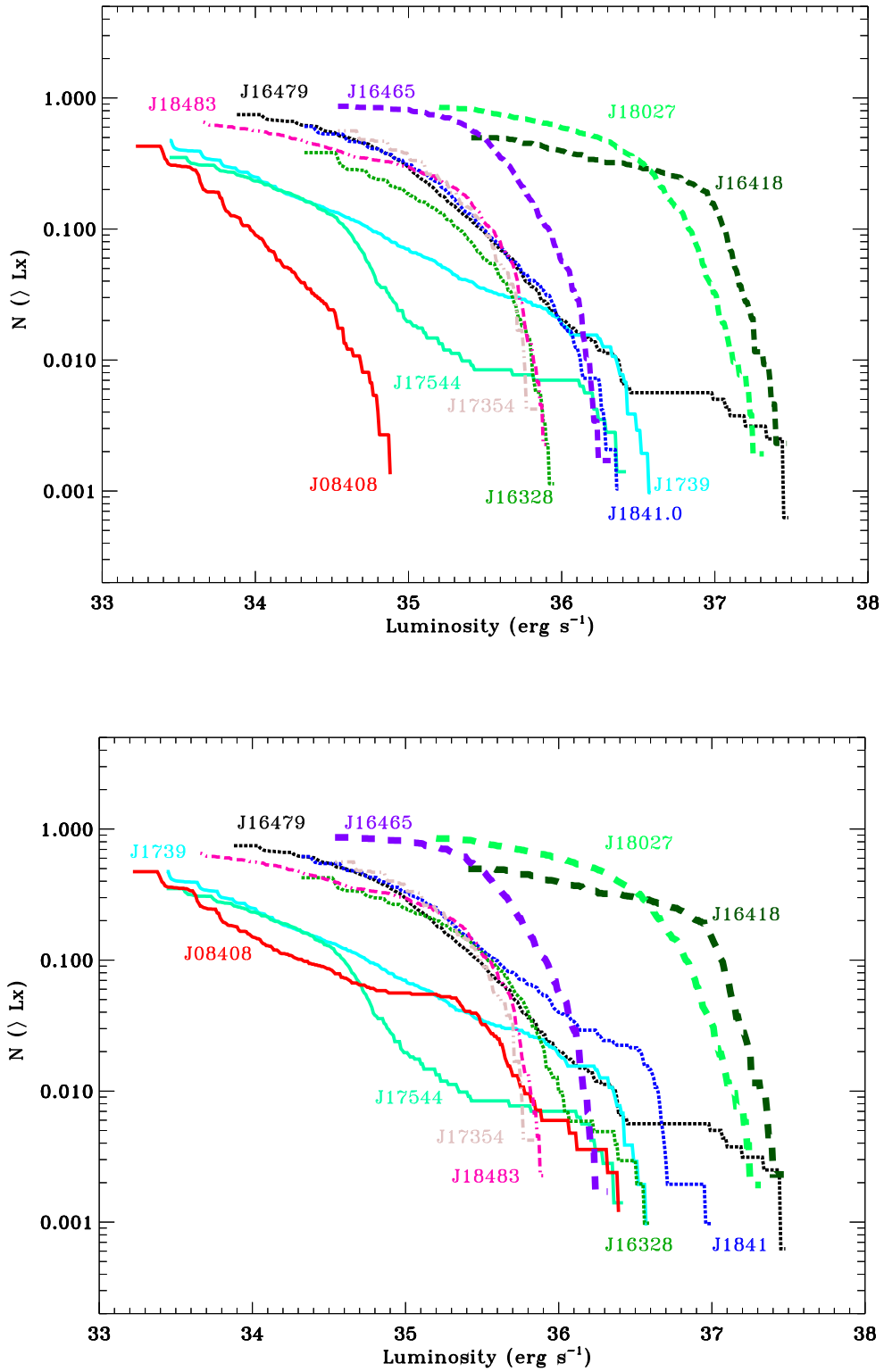

Figure 5: *Left*: cumulative luminosity distributions of all sources considered in this work (see Table 1). The distributions are constructed in the 2-10 keV energy band (see Sect. 3) but using only XRT data collected during the monitoring campaigns of all sources. *Right*: same as for the figure on the left, but in this case we also considered for the sources IGR J08408−4503, IGR J16328−4726, and AX J1841.0−0536 the outbursts recorded by XRT outside the corresponding monitoring campaigns. In both cases we represented the cumulative luminosity distributions of classical SgXBs with thicker dashed lines (including IGR J16418−4532 and IGR J16465−4507, as detailed in Sect. 3), and used dot-dashed lines for the intermediate SFXTs. The distributions of SFXTs have been represented with dotted lines, while solid lines have been used for the three most extreme SFXTs IGR J08408−4503, XTE J1739-302, and IGR J17544-2619.

- the cumulative luminosity distributions of the SFXT prototypes IGR J17544-2619, XTE J1739-302, and IGR J08408-4503 are shifted to even lower luminosities than other sources in this class. These three objects also display somewhat more complex profiles, and the identification of a knee is not trivial as in all other cases. We used solid lines in Fig. 5 to represent the luminosity distributions of the three SFXT prototypes.

Given the complex variety of all the cumulative distribution profiles, we did not attempt to fit them with some phenomenological model (e.g. a single or broken power-law). Instead, we show below how the shape of these profiles gives precious insights on the physical mechanisms regulating the X-ray activity of classical SgXBs and SFXTs.

4. Discussion and conclusions

In this paper, we made use of the long-term monitoring observations performed with the XRT on-board *Swift* to construct for the first time the cumulative luminosity distributions of most of the currently known SFXTs and a few classical SgXBs. Because of the re-classification of the sources IGR J16418-4532 and IGR J16465-4507, the cumulative luminosity distribution of three classical SgXBs can be presently constructed by using XRT data. The profile of these distributions closely resembles those of other classical SgXBs monitored in the hard X-rays and reported by P14 (see, e.g, the cases of Vela X-1 and 4U 1700-377). This similarity suggests that the cumulative distributions of all classical SgXBs is generally characterized by a profile featuring a single-knee. The latter occurs at luminosities of $\sim 10^{36}$-10^{37} erg s^{-1}.

Single-knee profiles can be relatively well understood in terms of wind accretion from an inhomogeneous medium. Fürst et al. (2010) showed that the X-ray luminosity of a system in which the NS is accreting from a highly structured medium, rather than a smooth wind, is expected to have a typical log-normal distribution. The profile of the corresponding cumulative distribution would thus be characterized by the presence of a single knee. Structures in the winds of a supergiant star are usually associated with "clumps", i.e. regions endowed with larger densities (a factor of $\sim$10) and different velocities (a factor of few) with respect to the surrounding medium (Owocki et al., 1988). These structures can be as large as $\sim$0.1 R_* (here R_* is the radius of the supergiant star; see, e.g., Dessart & Owocki, 2002, 2003, 2005; Šurlan et al., 2013). According to the classical picture of wind accreting systems (see, e.g., Frank et al., 2002, and references therein), the variation in the local density and/or velocity around a compact object produced by a clump can give rise to rapid changes in the mass accretion rate and thus on the released X-ray luminosity. Accretion from a moderately clumpy wind can thus qualitatively explain the X-ray variability of SgXBs and the profile of their cumulative luminosity distributions.

Oskinova et al. (2012) showed that, despite the remarkable variations in the X-ray luminosity that can be produced by accretion from a highly inhomogeneous medium, the long-term averaged luminosity of the system is comparable to that obtained in the case of a smoothed-out wind. It is thus expected that the position of the knee in the cumulative luminosity distribution of a SgXB, being roughly associated to the value of its averaged X-ray luminosity, will mainly depend on its orbital period: the closer the NS to its companion, the higher the expected averaged X-ray luminosity[3] (due to the enhanced density and slower velocity of the wind). This trend seems to be qualitatively respected by the classical SgXBs in our Fig. 5 and in Fig. 1 of P14. As an example, the knee of IGR J16418-4532, which is characterized by an orbital period of 3.4 days, is located at a higher luminosity with respect to that of IGR J18027-2016, which has a larger orbital period (4.5 days). The same is true if the comparison is carried out between IGR J18027-2016 and Vela X-1 (orbital period 8.9 days), and if the even larger orbital period of IGR J16465-4507 is taken into account. Additional XRT monitoring observations of classical SgXBs are currently being planned in order to confirm these findings.

According to the discussion above, it is unlikely that a simplified accretion wind scenario including only the presence of clumps could explain the X-ray behavior observed from the SFXT sources. Clumps provide, in principle, the means to trigger SFXT outbursts, but they cannot account for the substantial lower luminosity of these sources compared to classical SgXBs. To corroborate this argument, we first consider the cumulative distributions of the intermediate SFXTs IGR J18483-0311 and IGR J17354-3255, which are thought to be the missing link between classical systems and the SFXT prototypes. The profile of the distributions displayed by these two sources are similar to those of classical SgXBs, but are shifted toward the lower left side of the plots in Fig. 5. As an example, IGR J17354-3255 is characterized by an orbital period close to that of Vela X-1, but its average X-ray luminosity is a factor of $\sim$10 lower (see Fig. 1 in P14). This problem worsens when the cumulative luminosity distributions of the other SFXTs are considered. All SFXTs observed by XRT appear to be on-average much less luminous than the classical SgXBs. It is particularly worth mentioning the case of IGR J16479-4514 which has an orbital period similar to that of IGR J16418-4532 but its luminosity distribution is shifted at an average luminosity that is roughly a factor of $\sim$100 lower. The same conclusion would be reached by comparing the SFXT prototype IGR J17544-2619 with IGR J18027-2016 which have similar orbital periods (note that the relatively small uncertainties on the distance to all sources considered here would not be able to compensate for the estimated differences in luminosity; see Table 6 in R14). Beside being characterized by the lowest average luminosity, the three SFXT prototypes show also cumulative luminosity distributions with relatively complex profiles. In these cases, it is not trivial to accurately identify the main knee of their distribution.

It is interesting to note that the distributions of all SFXTs in Fig. 5 would clearly lead to low activity DCs for these objects

[3] We neglected here the eccentricity, photo-ionization of X-rays on the supergiant wind and other processes that can affect the overall X-ray luminosity (see, e.g., Ducci et al., 2010, and references therein). A detailed treatment of these effects is beyond the scope of the present paper.

when observed through low sensitivity large FoV instruments[4]. The latter are, indeed, not able to probe the rapid increases of the cumulative luminosity distributions of these sources in their fainter luminosity states, thus permitting us to study only the power-law shaped decay above $\gtrsim 10^{35}$ erg s^{-1} (see P14).

The mass loss rate of supergiants is known to have a significant spread depending on the star properties (Vink et al., 2000; Puls et al., 2008). However, the fact that all SFXTs are characterized by similar companion stars to those in classical SgXBs (Rahoui & Chaty, 2008) but are significantly subluminous compared to them, suggests a difference in the accretion processes on-going in these sources rather then a systematic discrepancy in the physical properties of their stellar winds (e.g., clumping factors). In order to produce a large decrease in the long-term X-ray luminosity, a mechanism is required to inhibit at least part of the accretion toward the NS and regulate plasma entry within the compact star magnetosphere. Theoretical models suggested so far to interpret the X-ray variability of SFXTs provide different ways to account for this feature.

In the models proposed by Grebenev & Sunyaev (2007) and Bozzo et al. (2008), the inhibition of accretion is provided by the onset of centrifugal and/or magnetic barriers. The latter are due to the rotation and magnetic field of the NS. Depending on the strength of this field and the value of the spin period, the onset of different accretion regimes can lead to a substantial variation of the overall source luminosity (a factor of 10^4-10^5). The switch from one regime to another is triggered by the interaction of the NS with moderately dense clumps. Assuming typical parameters of supergiant star winds, the largest variability is achieved when the magnetic barrier is at work. The latter requires intense magnetic fields ($\gtrsim 10^{14}$ G) and long spin periods ($\gtrsim$1000 s). While the magnetic gating would easily provide the means to achieve an X-ray variability comparable to that shown by the SFXT prototypes, the recent discovery of a cyclotron line at $\sim$17 keV from IGR J17544-2619 (suggesting a NS magnetic field intensity as low as B$\simeq 10^{12}$ G) raised questions on the applicability of the magnetic gating model at least to this source (Bhalerao et al., 2014).

In the quasi-spherical settling accretion model proposed by Shakura et al. (2012), the inhibition of accretion is provided by a hot quasi-static shell that forms above the NS magnetosphere when a sufficiently low mass accretion rate is maintained. A substantial average reduction (a factor of $\sim$30) of the mass accretion rate onto the NS (and thus X-ray luminosity) is expected if the plasma entry through the compact star magnetosphere from the shell is regulated by inefficient radiative plasma cooling. If Compton cooling dominates, a reduction of the mass accretion rate by a factor of $\sim$3 is achieved (Shakura et al., 2013). The bright SFXT flares are proposed to result from sporadic reconnections between the NS magnetosphere and the magnetic field embedded in the stellar wind. According to this model, the main difference between SgXBs and SFXTs would thus be that only for the latter sources the wind properties are such that a low density is stably maintained around the compact object (e.g., through a systematically lower mass loss rate from the supergiant star or higher/lower wind velocity/density) and magnetized stellar winds play a role in triggering large accretion episodes (Shakura et al., 2014). However, such requirements are difficult to accommodate, given the lack of any clear evidence of systematic differences between stellar winds in SFXTs and classical SgXBs (see Sect. 1). Further theoretical studies are currently on-going to investigate these issues.

Finally we note that the cumulative luminosity distributions of the SFXT prototypes reported in Fig. 5 feature the presence of plateau and multiple knees and thus look more complex than the profiles of other SFXTs and classical systems. At present we cannot exclude that these plateau are due to the relatively low number of bright SFXT outbursts recorded by XRT, which limits the completeness of the cumulative distributions at the higher luminosities ($\gtrsim 10^{36}$ erg s^{-1}; see also R14). In case future outbursts detected by XRT during our monitoring campaigns will be discovered to span a relatively large range in luminosity at the peak (e.g., a factor of 10 or more in the same time bin considered here), the decay of the cumulative luminosity distributions could be significantly affected (this would not change the sub-luminosity problem discussed before). However, it is noteworthy that the $\sim$12 years monitoring campaigns carried out with the *RXTE*/PCA on several SFXTs also feature plateau. Although the plateau in the PCA data are less prominent than those observed by XRT, in both cases these features are due to the brightest SFXT outbursts which are detected as rare events and span a relatively limited range in luminosity (Smith et al., 2012). If consolidated by future XRT monitoring observations, this could be interpreted in terms of those peculiar source states discussed above during which the highest mass accretion rate is achieved.

We conclude that the currently available XRT data provide support in favor of the general features of the theoretical models proposed so far to interpret the SFXT behavior, but do not allow yet to distinguish between them. A number of open questions remain to be investigated theoretically in the near future, including the requirement of strong magnetic fields for the applicability of the magnetic gating and the need for systematic differences in stellar wind parameters in the settling accretion model.

[4]The sensitivity limit is different for each source, as it depends on the intrinsic flux and the exposure time considered. We refer the reader to P14 for an exhaustive discussion regarding the ISGRI sensitivity limits for the observations of SFXTs.

Acknowledgments

The authors thank three anonymous referees for their valuable comments and suggestions. E.B. acknowledges support from ISSI through funding for the International Team meeting on "Unified View of Stellar Winds in Massive X-ray Binaries" (ID 253), during which most of the ideas presented in this paper were developed. PR acknowledges contract ASI-INAF I/004/11/0. LD thanks Deutsches Zentrum für Luft und Raumfahrt (Grant FKZ 50 OG 1301). The XRT data were obtained through ToO observations (2007-2012; contracts ASI-INAF I/088/06/0, ASI-INAF I/009/10/0) and through the contract ASI-INAF I/004/11/0 (2011-2013, PI P. Romano).

References

Bhalerao, V, Romano, P, Tomsick, J., Natalucci, L., Smith, D. M., et al. 2014, submitted to MNRAS(arXiv:1407.0112)

Barthelmy, S. D., Barbier, L. M., Cummings, J. R., et al. 2005, Space Sci. Rev., 120, 143

Bozzo, E., Romano, P., Ferrigno, C., Esposito, P., & Mangano, V. 2013, Advances in Space Research, 51, 1593

Bozzo, E., Stella, L., Israel, G., Falanga, M., & Campana, S. 2008, MNRAS, 391, L108

Bozzo, E., Falanga, M., & Stella, L. 2008, ApJ, 683, 1031

Burrows, D. N., Hill, J. E., Nousek, J. A., et al. 2005, Space Sci. Rev., 120, 165

Chaty, S. 2013, Advances in Space Research, 52, 2132

Dessart, L. & Owocki, S. P. 2002, A&A, 383, 1113

Dessart, L. & Owocki, S. P. 2003, A&A, 406, L1

Dessart, L. & Owocki, S. P. 2005, A&A, 437, 657

Drave, S. P., Bird, A. J., Sidoli, L., et al. 2013, MNRAS, 433, 528

Ducci, L., Sidoli, L., & Paizis, A. 2010, MNRAS, 408, 1540

Ducci, L., Romano, P., Esposito, P., et al. 2013, A&A, 556, A72

Ducci, L., Doroshenko, V., Romano, P., Santangelo, A., & Sasaki, M. 2014, A&A, 568, 76

Evans, P. A., Beardmore, A. P., Page, K. L., et al. 2009, MNRAS, 397, 1177

Frank, J., King, A., & Raine, D. J. 2002, Accretion Power in Astrophysics: Third Edition

Fürst, F., Kreykenbohm, I., Pottschmidt, K., et al. 2010, A&A, 519, A37

Gehrels, N., Chincarini, G., Giommi, P., et al. 2004, ApJ, 611, 1005

Giunta, A., Bozzo, E., Bernardini, F., et al. 2009, MNRAS, 399, 744

Grebenev, S. A. & Sunyaev, R. A. 2007, Astronomy Letters, 33, 149

Hill, A. B., Walter, R., Knigge, C., et al. 2005, A&A, 439, 255

Krimm, H. A., Holland, S. T., Corbet, R. H. D., Pearlman, A. B., Romano, P., et al. 2013, ApJS, 209,14

Lebrun, F., Leray, J. P., Lavocat, P., et al. 2003, A&A, 411, L141

Liu, Q. Z., van Paradijs, J., van den Heuvel, E. P. J. 2006, A&A, 455, 1165

Liu, Q. Z., Chaty, S., Yan, J. Z. 2011, MNRAS, 415, 3349

Mason, A. B., Norton, A. J., Clark, J. S., Negueruela, I., & Roche, P. 2011, A&A, 532, A124

Negueruela, I., Smith, D. M., Reig, P., Chaty, S., & Torrejón, J. M. 2006, in ESA Special Publication, Vol. 604, The X-ray Universe 2005, ed. A. Wilson, 165

Owocki, S. P., Castor, J. I., & Rybicki, G. B. 1988, ApJ, 335, 914

Oskinova, L. M., Feldmeier, A., & Kretschmar, P. 2012, MNRAS, 421, 2820

Paizis, A. & Sidoli, L. 2014, MNRAS, 439, 3439

Puls, J., Vink, J. S., & Najarro, F. 2008, A&A Rev., 16, 209

Rahoui, F. & Chaty, S. 2008, A&A, 492, 163

Romano, P., Krimm, H. A., Palmer, D. M., et al. 2014a, A&A, 562, A2

Romano, P., Ducci, L., Mangano, V., et al. 2014b, A&A, 568, A55

Romano, P., La Parola, V., Vercellone, S., et al. 2011, MNRAS, 410, 1825

Romano, P., Sidoli, L., Cusumano, G., et al. 2009, MNRAS, 399, 2021

Sguera, V., Bazzano, A., Bird, A. J., et al. 2006, ApJ, 646, 452

Shakura, N., Postnov, K., & Hjalmarsdotter, L. 2013, MNRAS, 428, 670

Shakura, N., Postnov, K., Kochetkova, A., & Hjalmarsdotter, L. 2012, MNRAS, 420, 216

Shakura, N., Postnov, k., Sidoli, L., & Paizis, A. 2014, MNRAS in press (arXiv:1405.5707)

Sidoli, L., Romano, P., Mangano, V., et al. 2008, ApJ, 687, 1230

Smith, D. M., Markwardt, C. B., Swank, J. H., & Negueruela, I. 2012, MNRAS, 422, 2661

Torrejón, J. M., Schulz, N. S., Nowak, M. A., Kallman, T. R. 2011, ApJ, 715, 947

Ubertini, P., Lebrun, F., Di Cocco, G., et al. 2003, A&A, 411, L131

Šurlan, B., Hamann, W.-R., Aret, A., et al. 2013, A&A, 559, A130

Vink, J. S., de Koter, A., & Lamers, H. J. G. L. M. 2000, A&A, 362, 295

Walter, R., Zurita Heras, J., Bassani, L., et al. 2006, A&A, 453, 133